Robotic Tissue Tracking for Beating Heart Mitral Valve Surgery

Shelten G. Yuen[a], Nikolay V. Vasilyev[b], Pedro J. del Nido[b], Robert D. Howe[a,c,1,*]

[a]*Harvard School of Engineering and Applied Sciences, 29 Oxford Street, Cambridge, MA, 02138, USA*
[b]*Department of Cardiovascular Surgery, Children's Hospital Boston, MA, USA*
[c]*Harvard-MIT Division of Health Sciences & Technology, Cambridge, MA, USA*

Abstract

The rapid motion of the heart presents a significant challenge to the surgeon during intracardiac beating heart procedures. We present a 3D ultrasound-guided motion compensation system that assists the surgeon by synchronizing instrument motion with the heart. The system utilizes the fact that certain intracardiac structures, like the mitral valve annulus, have trajectories that are largely constrained to translation along one axis. This allows the development of a real-time 3D ultrasound tissue tracker that we integrate with a 1 degree-of-freedom (DOF) actuated surgical instrument and predictive filter to devise a motion tracking system adapted to mitral valve annuloplasty. *In vivo* experiments demonstrate that the system provides highly accurate tracking (1.0 mm error) with 70% less error than manual tracking attempts.

Keywords: 3D ultrasound, real-time tissue tracking, motion compensation, medical robotics, beating heart surgery

1. Introduction

Beating heart surgery is a promising alternative to conventional procedures performed on the stopped heart (Angelini et al., 2002). This approach not only avoids the morbidities associated with the use of cardiopulmonary bypass (Zeitlhofer et al., 1993; Murkin et al., 1999; Bellinger et al., 1999), but also allows the surgeon to judge the efficacy of the procedure while the heart continues working. This is useful in the repair of structures like the mitral valve that open and close in response to changing pressure gradients during the heart cycle (Gersak, 2003). However, recent off-pump animal trials indicate that beating heart modification of the mitral valve cannot be performed reliably due to its fast motion (Downing et al., 2002; von Segesser et al., 2003) which ex-

ceeds the approximately one Hz tracking bandwidth of humans (Falk, 2002; Jacobs et al., 2003).

A robotic tracking system could assist the surgeon in this setting by synchronizing the motion of the instrument with the motion of the heart. This approach has been studied for coronary artery bypass graft procedures using multiple degree-of-freedom (DOF) robots and exploiting near periodicity in heart motion to track the external heart wall (Ginhoux et al., 2005; Bebek and Cavusoglu, 2007). Operating on the mitral valve includes additional challenges from working inside the heart. First, space restrictions make using a multi-DOF robot difficult. Second, an imaging technology that can image inside the heart at real-time rates must be used for robot guidance.

In this work, we consider the use of 3D ultrasound because it is capable of imaging tissue through blood while providing essential spatial information to guide complex intracardiac procedures which is not available in traditional 2D ultrasound images (Cannon et al., 2003). Although other imaging modalities like 3D computed tomography and magnetic resonance imaging offer higher

---

*Corresponding author.
Email address: howe@seas.harvard.edu (Robert D. Howe)
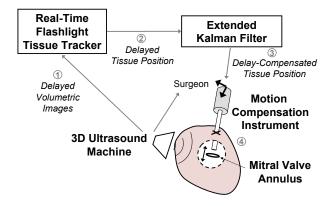*URL:* www.biorobotics.harvard.edu (Robert D. Howe)

Figure 1: The motion compensation system uses 3D ultrasound imaging to automatically synchronize the motion of an actuated, handheld surgical instrument with a tissue target. Circled numbers indicate the order of data flow through the system (1–3) and the resultant tracking position of the motion compensation instrument (4).
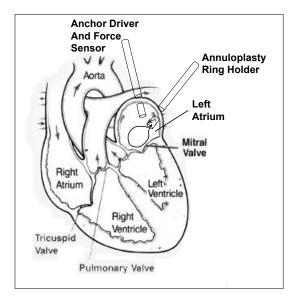

Figure 2: The prototype beating heart mitral valve annuloplasty uses two instruments inserted through the left atrial appendage. One instrument deploys anchors that secures a stiff ring to the annulus to reshape it. Note that the anchor driver approaches along the valves axis, which corresponds to the valves major component of motion.

spatial resolution, they have prohibitively slow imaging speeds, require special facilities, incur high costs, and cannot be moved into a standard operating room. In contrast, 3D ultrasound is relatively cheap, portable, and operates in real-time (25–30 Hz). 3D ultrasound is also becoming the preferred imaging technology among cardiac surgeons for guiding intracardiac beating heart repairs (Suematsu et al., 2004, 2005; Vasilyev et al., 2006, 2008) and it is advantageous to use it in the system to reduce training and the need for additional imaging equipment.

In our previous work, we showed that position-based eye-to-hand 3D ultrasound servoing of a handheld, 1 DOF motion compensation robot can enhance surgical task performance for beating heart mitral valve annuloplasty (Yuen et al., 2009); however, the system used a robot whose size limited surgical access into the heart and whose weight led to user fatigue. The system was also limited to tracking X-shaped fiducial targets in 3D ultrasound. A system suitable for intracardiac surgery must have real-time tissue tracking capabilities to guide the surgical instrument.

In this work, we present a new 3D ultrasound-guided motion compensation system for use in beating heart intracardiac procedures. The system builds on our previous work (Yuen et al., 2009) with a new, real-time 3D ultrasound tissue tracker and a miniaturized surgical robot that

can be used in the operating room. The guiding principle behind the new system is to leverage the surgeon's proficiency at aiming the instrument toward the desired surgical site, then to automatically track the tissue in front of the instrument under 3D ultrasound guidance. This approach is suited to our application because the mitral valve annulus has a predominantly uniaxial motion trajectory (Yuen et al., 2009). This enables the development of a novel, real-time tissue tracker that is robust to ultrasound noise because it draws on the high spatial coherence of the instrument to locate the tissue target. It also permits the design of a light, handheld motion compensation instrument with sufficient bandwidth to track the mitral valve annulus. In the following we describe this system and its components, then validate its performance in experiments conducted in a water tank and an *in vivo* Yorkshire pig beating heart model.

2

2. Methods and Materials

2.1. 3D Ultrasound-Guided Motion Compensation System

The motion compensation system assists the surgeon by following intracardiac structures that undergo rapid movement primarily in a single direction. As shown in our previous work, this includes the motion of the mitral valve annulus (Yuen et al., 2009). The system in this work builds on the system developed by Yuen et al. (2009) but incorporates a new tissue tracker that we term the "flashlight" tracker that can track arbitrary tissue targets in real-time 3D ultrasound. This is integrated with a miniaturized version of the actuated, handheld 1 DOF motion compensation instrument and predictive extended Kalman filter used by Yuen et al. (2009). A block diagram of the resulting system is shown in Fig. 1. The flashlight tissue tracker supplies measurements to the filter which, in turn, provides the reference trajectory for a PID controller to command the instrument. The surgeon designates the desired surgical site by aiming the tip of the instrument toward it.

Fig. 2 illustrates the surgical procedure that we are prototyping to perform beating heart mitral annuloplasty using this system. In the procedure, the motion compensation instrument is inserted through the left atrial appendage and aimed toward the mitral annulus. A custom annuloplasty ring is inserted through an adjacent incision and positioned by the surgeon. The instrument is tipped with a modified 14 gauge needle (OD 2.108 mm) that deploys surgical anchors (Vasilyev et al., 2006) to attach the ring to the annulus. The surgeon maneuvers the ring and anchor driver to appropriate locations over the annulus and deploys the anchors to secure the ring and reshape the annulus.

Preliminary experiments on freshly excised porcine heart indicate that a contact force of 2-3 N is required to deploy the anchor firmly into the annulus, but that forces must stay below 5.5 N to avoid tissue damage. This can be difficult to achieve when operating on moving heart tissue. The system described in this paper actuates the surgical instrument to compensate for heart motion to allow anchors to be deployed into the moving annulus. To do so, the instrument must be able to match the maximum annulus speeds and accelerations of 210 mm s^{-1} and 3.8 m s^{-2} (respectively) and have a 20 mm range of motion (Yuen
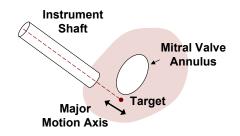

Figure 3: Real-time tracking of the surgical target is achieved by projecting along the instrument shaft until it intersects cardiac tissue.

et al., 2009). In order to synchronize instrument motion with that of the annulus, the system must also be able to automatically track the location of the annulus using 3D ultrasound while overcoming the latencies inherent to this imaging modality (Novotny et al., 2007).

2.1.1. Real-Time 3D Ultrasound "Flashlight" Tissue Tracker

Segmenting and tracking the mitral valve annulus in 3D ultrasound is inherently difficult due to noisy imaging and poor shape definition (Noble, 2006). Furthermore, the requirement for real-time (25–30 Hz) processing constrains the computation time available per volume. Rather than track the entire annular structure, we instead propose to track the tissue that the instrument is pointed toward. This simplification is clinically motivated: at any given moment, the surgeon only interacts with the small region of annulus directly in front of the instrument. Our approach allows the tracker to take advantage of the high spatial coherence of the instrument, which appears as a bright and straight object in the volume, to locate an otherwise poorly defined anatomical target. In this way the instrument is similar to a flashlight that highlights the tissue target (Fig. 3).

Fig. 4 charts the data flow in the flashlight tracker. It consists of two consecutive operations: instrument detection followed by target segmentation. We employ the modified Radon transform for real-time detection of the ray that passes through the central axis of the instrument shaft in 3D ultrasound (Novotny et al., 2007). Next, we turn to distinguishing between the target and instrument along this ray. We construct a 2D image slice through the ultrasound volume that contains the instrument shaft (Fig. 5A-B). Pixels in the slice that exceed a
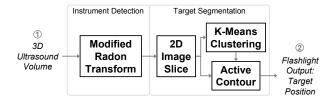
3

Figure 4: Data processing chain in the flashlight real-time tissue tracker. Instrument detection is performed using the full 3D ultrasound volume. Subsequent target segmentation is done on a 2D image slice through the volume along the instrument shaft. The target is taken as the tissue directly in front of the instrument. Circled numbers correspond to those shown in Fig. 1.

grayscale intensity threshold I_t are grouped into two clusters based on Euclidean distance using the K-means algorithm (Afifi et al., 2004). The value of I_t is empirically chosen to remove noise and the mitral leaflets from the clustering. The resulting clusters roughly coincide with the locations of the instrument and tissue target (Fig. 5C-D). *A priori* knowledge of the ultrasound probe placement relative to the instrument and the tissue allows us to designate the more distal cluster as the target. However, the cluster location for the target may be imperfect when the instrument and tissue are close to each other because the two K-means clusters can interfere with one another (Fig. 5D).

To handle this case, a final step is performed using an active contour to segment the target surface (Fig. 5E-F). The active contour is initialized by radially projecting n points from the center of the K-means target cluster until they reach a pixel intensity lower than I_t. The active contour is governed by the minimization of the energy equation

$$E = \int_S (\alpha E_{\text{elastic}} + \beta E_{\text{bending}} + \gamma E_{\text{image}})dS. \qquad (1)$$

The energy consists of an elastic term that encourages uniform point spacing on the contour, a bending term that penalizes high curvature, and an image gradient term that forces the active contour toward edges. The parameters α, β, and γ are chosen to balance the relative contributions of each term. Real-time minimization of (1) is achieved through a greedy algorithm with point neighborhoods based on 8-connectivity (Willams and Shah, 1992). The first intersection point of the contour with the ray along the instrument shaft is taken as the target position.

Examples of the tissue segmentation steps are shown in Fig. 5 for two cases where the instrument is far and close to the target. Note that the use of an active contour makes target segmentation robust to cases where the instrument is near the target.

2.1.2. Time Delay Compensation

Although the flashlight tissue tracker operates in real-time, there are latencies in the system that must be removed prior to commanding the motion compensation instrument. The acquisition and transfer of ultrasound volumes requires ≈30 ms and the subsequent detection of the instrument takes an additional ≈30 ms (Novotny et al., 2007). For comparison, the mitral valve annulus traverses over half of its trajectory in 60 ms at the onset of ventricular relaxation.

As in previous work, we compensate for time delay by exploiting the nearly periodic motion of the heart to predict the tissue trajectory into the near future (Yuen et al., 2009). Briefly, we model the target trajectory as an *m*-harmonic, time-varying Fourier series with an offset

$$x(t) = c(t) + \sum_{i=1}^{m} r_i(t)\sin(\theta_i(t)). \qquad (2)$$

We estimate the parameters of this model using an extended Kalman filter (EKF). Because it is recursive, it is amenable to a real-time implementation. It has the added benefit of providing noise reduction to the estimated target trajectory through the regularization of the flashlight tracker measurements against the motion model in (2).

We note that the explicit modeling of heart motion as quasiperiodic in (2) enables this method to adapt quickly to normal variations in heart rate (Yuen et al., 2009). This does not extend to cases of arrhythmia, in which the motion of the heart is inherently unpredictable. For these cases, the system could be augmented to include electro-cardiography to predict arrhythmia at about 90 ms prior to onset, allowing the robot to go into a failsafe mode (Cuvillon et al., 2006). If severe arrhythmia is present during surgery, it may also be mitigated medically by treating the patient with beta blockers and electrically pacing the heart to a fixed rate.

2.1.3. Motion Compensation Instrument

The motion compensation instrument is a handheld surgical anchor deployment device that actively cancels the
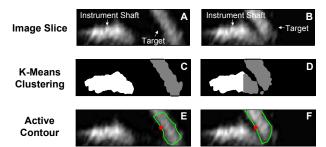
4

Figure 5: Outputs from each tissue segmentation step for examples where the instrument is far and near the target (left and right columns, respectively). The image slice through the instrument is shown in the top row. K-means clusters are shown as white and gray objects in the middle row. The segmented target shape (line) and tracking point (dot) are shown in the bottom row.
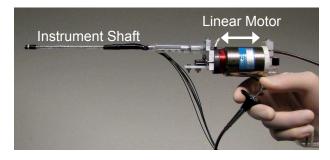

Figure 6: The motion compensation instrument is a 1 DOF actuated anchor driver instrument that is capable of tracking fast intracardiac structures.

dominant 1D motion component of the mitral valve annulus. Fig. 6 shows the instrument. It is a miniaturized version of a previous design (Yuen et al., 2009). It incorporates a voice coil linear motor (NCC10-15-023-1X, H2W Technologies, Valencia, CA, USA) for actuation of the anchor deployment stage up to speeds and accelerations of 1.49 m/s and 103 m/s^2 with a 25 mm range of motion. A high linearity potentiometer (P3 America, San Diego, CA, USA) provides position sensing. The instrument position is controlled with a slightly overdamped response by a 1 kHz PID servo loop and has a -3 dB point of 35.0 Hz (-40 dB/dec roll off rate). The overall weight of the instrument is 0.76 kg, which is less than 50% of the weight of the original. Weight reduction is achieved by using a smaller motor and light plastic materials for construction.

2.1.4. System Implementation

The motion compensation system uses a dual CPU AMD Opteron 285 2.6 GHz PC with 4 GB of RAM to process the ultrasound data and control the motion compensation instrument. A 3D ultrasound machine (Sonos 7500, Philips Healthcare, Andover, MA, USA) streams volumes at 28 Hz to the PC over a 1 Gb LAN using TCP/IP. A program written in C++ retrieves the ultrasound volumes and loads them onto a GPU (7800GT, nVidia Corp, Santa Clara, CA, USA) for real-time instrument axis detection. The GPU renders image slices through the instrument shaft that are rotated to be horizontal through a trilinear interpolation. Subsequent flashlight tissue tracking operations are done with a pixel intensity threshold of $I_t = 50$ and active contour parameters $n = 10, \alpha = 0.5, \beta = 0.5$, and $\gamma = 1.0$. Preliminary water tank experiments indicate that the flashlight tracker is robust to changes in I_t and the ratios between α, β, and γ up to or exceeding a factor of two. The EKF trains on 5 s of flashlight position data and feeds-forward a tissue trajectory 78 ms ahead (68 ms from image acquisition, transfer, and processing; 10 ms from instrument latency) to the 1 kHz PID servo loop controlling the motion compensation instrument. System timing is enforced by a callback driven by an external control card (PHANToM 1.5A PCI card, SensAble Technologies, Woburn, MA, USA). The instrument is powered by a BOP36-1.5 M linear power amplifier (Kepco, Flushing, NY, USA). Real-time tissue tracking, predictive filtering, and control algorithms are executed on the CPU. The same system parameters were used for both water tank and *in vivo* testing.

2.2. Experimental Validation

We conducted two sets of experiments to validate the proposed system. The first experiment assessed tracking accuracy in a water tank, enabling a characterization of the system and its subcomponents in a controlled environment. A second experiment was performed in the surgical setting to measure accuracy under *in vivo* noise conditions. This experiment also measured the accuracy of a surgeon attempting to track the annulus manually (i.e. without the motion compensation system) to roughly establish human capabilities in this task.
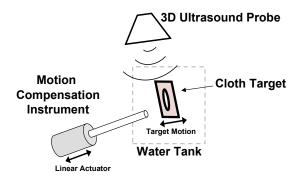
Figure 7: Tank experiment setup.

2.2.1. Tank Study

The tracking accuracy of the system was tested against a simulated mitral valve annulus target in a water tank. Fig. 7 depicts the setup. Annulus motion was simulated at 60 beats per minute (bpm) by a cam follower mechanism that replicates the dominant 1D motion component of the human mitral valve annulus, as done previously by Yuen et al. (2009). A cloth tissue phantom was mounted to the cam and positioned in the tank. The motion compensation instrument was aligned to within about 15° of the motion axis of the target. The ultrasound probe was positioned to simultaneously image the target and instrument and set approximately perpendicular to the target motion axis to match the expected probe placement conditions *in vivo*. A potentiometer measured target position for off-line assessment of system accuracy.

2.2.2. In Vivo Animal Study

In vivo validation was performed in a porcine beating heart model (Fig. 8). Motion tracking was conducted in two Yorkshire pigs during open chest, beating heart procedures. In both animal trials, the tip of the motion compensation instrument was inserted into the left atrial appendage and secured by a purse-string suture. The ultrasound probe was positioned epicardially on the left side of the heart and placed in a plastic bag with transmission gel to improve contact with the irregular surface of the heart. Because the probe was placed against the moving external wall of the heart, it underwent motions of approximately 2 mm during every heart cycle. Probe position also varied slowly over time because it was handheld.

The requirement of simultaneously imaging the instrument and the mitral valve restricted probe placement to between the left atrium and left ventricle. Also, as described by Novotny et al. (2007), it is not physically possible to image the instrument beyond a 60° angle with respect to the probe because of the dimensions and limited field of view of the probe. A large incidence angle also causes low signal strength for the instrument because the signal scatters away from the probe.

The surgeon was instructed to aim the instrument tip toward a point on the mitral valve annulus and orient the instrument shaft to align with the major motion axis of the annulus. During the second animal trial, the surgeon also attempted to manually track the annulus with a stationary, noncompensating instrument. The surgeon was given three practice attempts, followed by the actual trial. Motion tracking occurred for 20 s in each trial.

The 3D ultrasound images from the trials were recorded and manually segmented to evaluate tracking performance. For each time-stamped volume, at least ten points were selected for the cardiac tissue along the instrument axis. These were used to calculate the centroid of the tissue target over time. Points in the left ventricle and on the mitral leaflets were excluded. Segmentations were verified by a cardiac surgeon with expertise in 3D ultrasound imaging and beating heart surgery.

The experimental protocol was approved by the Children's Hospital Boston Institutional Animal Care and Use Committee. All animals received humane care in accordance with the 1996 *Guide for the Care and Use of Laboratory Animals*, recommended by the US National Institute of Health.

3. Results

Fig. 9 shows a representative water tank tracking example. Intermediate system outputs from the flashlight tracker and EKF are also overlaid and labeled with circled numbers that match those in Fig. 1. The motion compensation system provided instrument synchronization to the target with 1.8 mm RMS error (MCI vs. target traces in Fig. 9). Position measurements from the flashlight tracker had RMS errors of 2.5 mm and were delayed by a total of 68 ms due to 3D ultrasound volume acquisition and transfer time and instrument detection latency. Tissue segmentation in the tracker required less than 1 ms. The error and
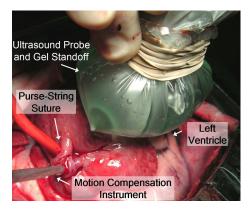
6

Figure 8: *In vivo* experiment setup.

Animal Trial No.	Tracking Condition	Heart Rate (bpm)	RMS Tracking Error (mm)
1	System	100	0.8
2	System	113	1.0
2	Manual	116	3.2

Table 1: *In vivo* tracking results for both animal trials. The second trial included tracking with and without the motion compensation system.

error while it beat at a spontaneous heart rate of 113 bpm. Qualitatively, the tracking does not mimic the target trajectory as faithfully as in the water tank case. A major contributor to this is the reduced imaging quality *in vivo*. Fig. 11 depicts the imaging conditions while tracking over one heart cycle. Imaging artifacts and dropout are evident. There is also a slow respiratory motion component that is unmodeled by the EKF that introduces a small tracking error (Fig. 10A).

The system provided RMS tracking errors less than or equal to 1.0 mm in both in vivo trials (Table 3). In contrast, manual tracking (Fig. 10B) yielded RMS errors of 3.2 mm on a slightly faster 116 bpm heart rate. The cross-correlation between the trajectories of the target and instrument in this case suggests that the surgeon lagged behind the target by approximately 339 ms. The RMS tracking error with this delay removed would be 1.3 mm.
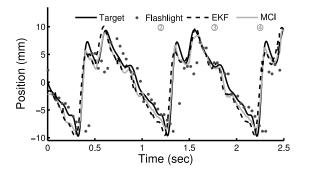

Figure 9: Water tank example of the system tracking a simulated mitral valve annulus target with the motion compensation instrument. Intermediate outputs from the flashlight tracker and the EKF are also shown. Flashlight tracker positions are delayed by 68 ms because of latencies in 3D ultrasound and image processing. Relative position offsets are removed for clarity. Circled numbers correspond to those shown in Fig. 1.

4. Discussion

These experiments are the first to show that robotic motion tracking of beating, intracardiac tissue is feasible in the surgical setting. Results from our *in vivo* study demonstrate that robotic tracking of the mitral valve annulus can be achieved with low 1.0 mm RMS error using standard 3D ultrasound imaging. This constitutes a 70% error reduction when compared to manual attempts. The flashlight tissue tracker proved to be robust to *in vivo* imaging artifacts, dropout, and noise by exploiting the spatial coherence of the instrument in ultrasound to pinpoint the tissue target. High accuracy motion tracking was achieved in the presence of significant delay and noise by regularizing position measurements against the cyclic motion of the heart with a predictive extended Kalman filter. Water tank results show that the filter reduces noise by 30% while simultaneously removing the overall system delay of 78 ms.

time delay in the flashlight measurements were mitigated by the EKF, yielding a feedforward target trajectory with 1.7 mm RMS error.

In vivo results indicate that the system provides accurate motion tracking under surgical conditions. Fig. 10A shows the tracking results for one of the *in vivo* trials[2]. Both the positions of the tissue target and instrument are shown. The system tracked the target with a 1.0 mm RMS

---

[2]This paper has a supplementary video that demonstrates the *in vivo* tracking viewed in 3D ultrasound at `http://www.biorobotics.harvard.edu/InVivo_MitralAnnulus_Tracking.avi` (1.6 MB).
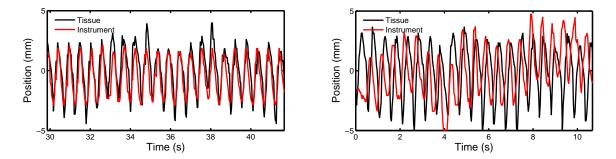
Figure 10: *In vivo* tracking examples conducted with the motion compensation system (A) and manually (B). The manual tracking example is the last and best attempt, after the surgeon had two training trials. The relative positional offsets between the instrument and tissue target are removed for clarity.
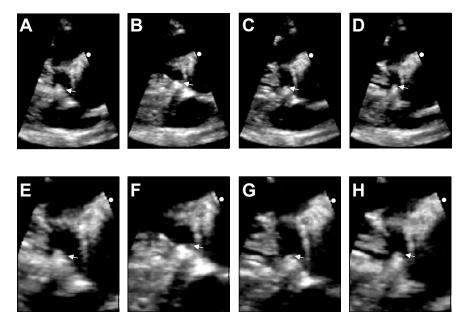

Figure 11: 3D ultrasound images of the motion compensation instrument tracking a region of the mitral valve annulus (arrows) in a beating porcine heart over one heart cycle. The base of the instrument shaft is denoted by a dot. Panels A–D (top row) show the entire field of view and panels E–H (bottom row) show corresponding magnified views of the instrument tip and target. The instrument tip is a cylindrical rod; however, the presence of ultrasound imaging artifacts distorts its appearance (Huang et al., 2007).

Prior research has shown that humans cannot track the heart when it is beating faster than 60 bpm (Falk, 2002; Jacobs et al., 2003). Our preliminary manual tracking result suggests that the main reason for this is the presence of a large lag that puts the instrument motion out of phase with the heart. For the cardiac surgeon in this study, we estimate this lag to be 339 ms on a heart beating at 116 bpm. This is consistent with the lags measured by Jacobs et al. (2003) for tasks against simulated heart motion at 35 and 60 bpm. A retrospective analysis of the manual tracking trial suggests that the surgeon was able to match the frequency and amplitude of the annular trajectory reasonably well – to 1.3 mm RMS error when corrected for the 339 ms lag. It is unlikely that training will reduce the lag to levels low enough to achieve accurate manual tracking: human visual processing requires roughly 150 ms (Thorpe et al., 1996) and, as discussed above, even a 60 ms delay is intolerable for motion compensation. The surgeon could conceivably predict the tissue trajectory and feedforward its motion like our strategy with the extended Kalman filter. However, even if possible, this would not be a clinically viable approach because it would severely limit the surgeon's ability to attend to the other aspects of the procedure.

The difficulty with manual heart tracking has inspired a number of parallel efforts in motion compensation for external heart procedures like coronary artery bypass graft. Nakamura et al. (2001) demonstrated automatic tracking of a laser point moving like the external heart wall with a 4 DOF robot guided by two high speed cameras. Later, Ginhoux et al. (2005) provided an in vivo demonstration with a modified 6 DOF AESOP robot guided by a high-speed camera to track LEDs affixed to a beating porcine heart. Similarly, Bebek and Cavusoglu (2007) used a 6 DOF PHANToM robot to track sonomicrometry sensors sutured to the heart surface. Because these systems function outside of the heart, they are able to achieve excellent results by using relatively large robots with fast (257–955 Hz) and accurate (250 μm–0.25 mm) positioning sensors that either track fiducials or are placed onto the surgical target.

Limited by the constraints of operating inside the heart, our system uses relatively low frequency (28 Hz), low accuracy (0.5 mm), high noise 3D ultrasound imaging to directly track heart tissue. We also adopt a simplified 1 DOF robot that can function within the restricted space of the heart. Using this system in a beating porcine heart, we show a 70% decrease in error compared to manual tracking. We anticipate a larger benefit in the human heart because the human mitral valve annulus undergoes a larger excursion (10–18 mm) (Wandt et al., 1997; Flachskampf et al., 2000; Yuen et al., 2009) than was seen in our porcine model here (6 mm). However, the current study suggests a potential improvement to the system by adding a low frequency term to the motion model in the filter. This may improve tracking the small, slowly-varying motion component seen in the *in vivo* result (Fig. 10A) that is due to respiration. A model predictive controller may also improve robotic tracking accuracy (Ginhoux et al., 2005; Bebek and Cavusoglu, 2007). However, as described in Section 3, the EKF prediction error is 1.7 mm RMS and the robot tracking error is 1.8 mm RMS – this indicates that the error contribution from the PID controller is small and only increases the overall error by 0.1 mm RMS. Future work using a low bandwidth, multi-DOF robot could employ model predictive control to enhance the tracking bandwidth. Its use for a 1 DOF, high bandwidth robot such as in the current system does not appear necessary given the performance achieved with a simple PID controller with feed-forward EKF predictions.

5. Acknowledgement

Afifi, A., Clark, V. A., May, S., 2004. Computer-Aided Multivariate Analysis, 4th Edition. Texts in Statistical Science. Chapman & Hall/CRC.

Angelini, G. D., Taylor, F. C., Reeves, B. C., Ascione, R., 2002. Early and midterm outcome after off-pump and on-pump surgery in beating heart against cardioplegic arrest studies (BHACAS 1 and 2): a pooled analysis of two randomised controlled trials. Lancet 359, 1194–1199.

Bebek, O., Cavusoglu, M., Jun. 2007. Intelligent control algorithms for robotic assisted beating heart surgery. IEEE Transactions on Robotics 23 (3), 468–480.

Bellinger, D., Wypij, D., Kuban, K., Rappaport, L., Hickey, P., Wernovsky, G., Jonas, R., Newburger, J., 1999. Developmental and neurological status of children at 4 years of age after heart surgery with hypothermic circulatory arrest or low-flow cardiopulmonary bypass. Circulation 100, 526–532.

Cannon, J. W., Stoll, J. A., Salgo, I. S., Knowles, H. B., Howe, R. D., Dupont, P. E., Marx, G. R., del Nido, P. J., 2003. Real-time three-dimensional ultrasound for guiding surgical tasks. Computer Aided Surgery 8 (2), 82–90.

Cuvillon, L., Gangloff, J., Mathelin, M. D., Forgione, A., 2006. Towards robotized beating heart tecabg: Assessment of the heart dynamics using high-speed vision. Computer Aided Surgery 11 (5), 267–277.

Downing, S. W., Herzog Jr., W. A., McLaughlin, J. S., Gilbert, T. P., 2002. Beating-heart mitral valve surgery: Preliminary model and methodology. Journal of Thoracic and Cardiovascular Surgery 123 (6), 1141–1146.

Falk, V., 2002. Manual control and tracking – a human factor analysis relevant for beating heart surgery. Annals of Thoracic Surgery 74, 624–628.

Flachskampf, F. A., Chandra, S., Gaddipatti, A., Levine, R. A., Weyman, A. E., Ameling, W., Hanrath, P., Thomas, J. D., 2000. Analysis of shape and motion of the mitral annulus in subjects with and without cardiomyopathy by echocardiographic 3-dimensional reconstruction. Journal of the American Society of Echocardiography 13 (4), 277–287.

Gersak, B., 2003. A technique for aortic valve replacement on the beating heart with continuous retrograde coronary sinus perfusion with warm oxygenated blood. Annals of Thoracic Surgery 76, 1312–1314.

Ginhoux, R., Gangloff, J., de Mathelin, M., Soler, L., Sanchez, M. M. A., Marescaux, J., 2005. Active filtering of physiological motion in robotized surgery using predictive control. IEEE Transactions on Robotics 21 (1), 27–79.

Huang, J., Vasiylev, N. V., Suematsu, Y., Cleveland, R. O., Dupont, P. E., 2007. Imaging artifacts of medical instruments in ultrasound-guided interventions. Journal of Ultrasound in Medicine 26, 1303–1322.

Jacobs, S., Holzhey, D., Kiaii, B. B., Onnasch, J. F., Walther, T., Mohr, F. W., Falk, V., 2003. Limitations for manual and telemanipulator-assisted motion tracking – implications for endoscopic beating-heart surgery. Annals of Thoracic Surgery 76, 2029–2035.

Murkin, J. M., Boyd, W. D., Ganapathy, S., Adams, S. J., Peterson, R. C., 1999. Beating heart surgery: why expect less central nervous system morbidity? Annals of Thoracic Surgery 68, 1498–1501.

Nakamura, Y., Kishi, K., Kawakami, H., May 2001. Heartbeat synchronization for robotic cardiac surgery. In: Proceedings of IEEE International Conference on Robotics and Automation (ICRA'01). pp. 2014–2019.

Noble, J. A., 2006. Ultrasound image segmentation: A survey. IEEE Transactions on Medical Imaging 25 (8), 987–1010.

Novotny, P. M., Stoll, J. A., Vasilyev, N. V., del Nido, P. J., Zickler, T. E., Dupont, P. E., Howe, R. D., 2007. GPU based real-time instrument tracking with three-dimensional ultrasound. Medical Image Analysis 11, 458–464.

Suematsu, Y., Martinez, J. F., Wolf, B. K., Marx, G. R., Stoll, J. A., DuPont, P. E., Howe, R. D., Triedman, J. K., del Nido, P. J., 2005. Three-dimensional echo-guided beating heart surgery without cardiopulmonary bypass: atrial septal defect closure in a swine model. Journal of Thoracic and Cardiovascular Surgery 130, 1348–1357.

Suematsu, Y., Marx, G., Stoll, J., Dupont, P., Cleveland, R., Howe, R., Triedman, J., Mihaljevic, T., Mora, B., Savord, B., Salgo, I., del Nido, P., 2004. Three-dimensional echocardiography-guided beating-heart surgery without cardiopulmonary bypass: A feasibility study. Journal of Thoracic and Cardiovascular Surgery 128 (4), 571–578.

Thorpe, S., Fize, D., Marlot, C., 1996. Speed of processing in the human visual system. Nature 381 (6582), 520–522.

Vasilyev, N., Martinez, J., Freudenthal, F., Suematsu, Y., Marx, G., del Nido, P., 2006. Three-dimensional echo

and videocardioscopy-guided atrial septal defect closure. Annals of Thoracic Surgery 82 (4), 1322–1326.

Vasilyev, N. V., Melnychenko, I., Kitahori, K., Freudenthal, F. P., Phillips, A., Kozlik-Feldmann, R., Salgo, I. S., del Nido, P. J., , Bacha, E. A., 2008. Beating heart patch closure of muscular ventricular septal defects under real-time three dimensional echocardiographic guidance: A preclinical study. Journal of Thoracic and Cardiovascular Surgery 135 (3), 603–609.

von Segesser, L. K., Tozzi, P., Augstburger, M., Corno, A., 2003. Working heart off-pump cardiac repair (OP-CARE) – the next step in robotic surgery? Interactive Cardiovascular and Thoracic Surgery 2, 120–124.

Wandt, B., Bojo, L., Wranne, B., 1997. Influence of body size and age on mitral ring motion. Clinical Physiology 17, 635–646.

Willams, D. J., Shah, M., Jan. 1992. A fast algorithm for active contours and curvature estimation. Computer Vision Graphics and Image Processing: Image Understanding 55 (1), 14–26.

Yuen, S. G., Kettler, D. T., Novotny, P. M., Plowes, R. D., Howe, R. D., 2009. Robotic motion compensation for beating heart intracardiac surgery. International Journal of Robotics Research 28 (10), 1355–1372.

Zeitlhofer, J., Asenbaum, S., Spiss, C., Wimmer, A., Mayr, N., Wolner, E., Deecke, L., 1993. Central nervous system function after cardiopulmonary bypass. European Heart Journal 14, 885–890.